18th Brazilian Congress of Thermal Sciences and Engineering
November 16-20, 2020, (online)

ENC-2020-0046
CFD INVESTIGATION OF A SUPERSONIC COMBUSTION CHAMBER OF A SCRAMJET ENGINE

João Vitor Marques Brito de Siqueira
Instituto Tecnológico de Aeronáutica – Praça Marechal Eduardo Gomes 50 – São José dos Campos, SP, 12228-900
joaovitormarques22@hotmail.com

Guilherme Borges Ribeiro
Instituto Tecnológico de Aeronáutica – Praça Marechal Eduardo Gomes 50 – São José dos Campos, SP, 12228-900
gbribeiro@ita.br

Abstract. *This work has the purpose of investigating, through detailed three-dimensional computational fluid dynamics (CFD) analyses, different physical phenomena in a scramjet combustor chamber. This work focuses on the analysis of contour images of Mach number, static pressure, temperature, moles of H_2o and H_2. Besides contour images, properties such as pressure and temperature along the upper and lower walls have also been investigated. Besides it, viscous effects due to the sidewall, and the influence these effects have on the airflow and combustion process, are also investigated.*
Keywords: *Scramjet, CFD, Mach number, Combustion chamber*

1. INTRODUCTION

During the 21st century, a great number of loads are assumed to be taken into orbit. The cost to put something into orbit is enormous and therefore the development of an air-breathing engine as an alternative for hypersonic propulsion is required. The great advantage air-breathing engines have is that they don`t need the vehicle itself to transport the oxygen for the combustion, as it happens to rocket engines. The use of air-breathing engines enables the vehicle to decrease its volume and weight resulting in higher specific impulses (Heiser, 1994; Segal, 2009; Griffiths, 2005; Smart, 2008; Alcaide, 2007). The supersonic combustion ramjet (scramjet) has been conceived to operate in high altitude flights. Its theoretical top speed is between Mach numbers 12 and 24 (Segal, 2009). The ramjet engine features combustion in subsonic flow while the scramjet engine has its fuel combustion happening with air at supersonic speed. That difference brings up some technological challenges to develop a scramjet engine. When the airflow is decelerated by the scramjet engine, the relative velocity and kinetic energy decrease, and conservation of energy requires that any missing kinetic energy will reappear as internal energy, with the result that pressure, temperature, and density of the flow entering the burner are considerably higher than in the freestream. When the flight Mach number exceeds about 6, this effect becomes so pronounced that it is no longer advantageous to decelerate the flow to subsonic speeds (Heiser, 1994). As in any conventional thermal power cycle, in both engines, the flow is compressed. The airflow compression is done by oblique shock waves at the inlet and diffuser. After such compression in ramjet engines, the airflow becomes subsonic after passing by a normal shock wave and inside the burner happens subsonic combustion. On the other hand, in scramjet engines, the airflow goes to the burner in supersonic speeds. If velocities are increased too much, the normal shock wave that occurs inside the ramjet engine leads to hugely high pressure loss. Yet the temperature increases a lot causing structural stresses and chemical dissociation of the airflow, which makes the cycle to lose energy (Smart, 2008). The solution for it is to remove the normal shock and allow the airflow to enter the combustor in supersonic speeds, from where comes the idea of the supersonic combustion ramjet, or scramjet. The fuel, in a scramjet engine, remains inside the burner for a really short time and therefore it is injected just downstream the diffuser to achieve a rapid and thorough mixing. Thus, the high pressure, hot flow is directed to the nozzle that, in the case of a scramjet engine, must be divergent once the airflow is supersonic. The after-combustion flow is then exhausted into de atmosphere and can also be accelerated by the vehicle after-body that can be used as an expansion surface. Scramjets are supposed to operate in hypersonic speeds, i.e. above Mach 5, and theoretical operational limits as high as Mach 24 (Segal, 2009).

The supersonic combustion in a scramjet engine represents one of the biggest challenges to develop a hypersonic vehicle. At first, the velocities throughout the engine, in the thousands of meters per second,

means that milliseconds only are available between the airflow to enter the combustor, to inject the fuel, achieve a fairly uniform mixture of air and fuel, ignite, burn properly and exhaust (Heiser, 1994). Mixing is complex. For example, combustion is impossible to be initiated until mixing is achieved at a molecular level. And in regions where the combustion happens, the temperature rise and the chemical composition changes modify the parameters responsible for mixing. (Segal, 2009). Besides it, this process needs to be carried out within a reasonable length and avoiding a normal shock waves inside the engine (Heiser, 1994). It is certainly not trivial to perform this kind of combustion. Scramjets for access-to-space systems demand combustion efficiency of at least 80% (Smart and Tetlow, 2009). These kind of scramjets are accelerated and then they require to operate in a high range of Mach numbers. The higher the velocities achieved the better for the scramjet to operate longer. In this way, as it is at such high velocities it becomes more and more difficult to generate the net thrust to accelerate the vehicle (Smart, 2008; Barth *et al*., 2009; Moule *et al*., 2014). The kinetic energy greatly increases as the airflow velocity goes up and therefore it becomes increasingly difficult to add energy to the flow through combustion. The ability to add energy to the air through combustion competes with the engine drag losses. At moderate hypersonic flight velocities, a significant quantity of heat can be added to the airflow without generating much engine drag losses. This results in higher acceleration capabilities. As the flight velocities go up the relative heat addition to the airflow progressively decreases while engine drag losses continuously increase until the drag equals the heat addition and the air-breathing-based system reaches the limits of its flight envelope (Segal, 2009). Having a longer combustor and so that the combustion process can continue until the efficiency is high enough to overcome the drag cannot be taken as an alternative solution. Drag in the combustor and nozzle is responsible for up to 60% of total skin friction drag in scramjets (Tanimizu e*t al*., 2009). Longer combustor results in more drag. Trial-and-error and empirical approaches have been sufficient to develop high-performance designs. However, for higher flow velocities, these techniques cannot be applied (Doherty *et al*., 2012).

The objectives of this work are investigating the physical phenomena inside the combustion chamber of a scramjet engine through contour images and distribution of properties on the walls. All the numerical calculations in this work used the fluid dynamics ANSYS Fluent code.

2. GOVERNING EQUATIONS

The classical Navier Stokes equations for compressible flow has been considered. For a time-dependent fluid flow, Eq.(2.1) represents the mass balance, Eq.(2.2) to Eq. (2.4) the momentum balances in the x, y and z directions, and Eq. (2.5) is the energy balance. In these equations, *u*, *v*, *w* refer to flow velocities in the x, y and z directions respectively. And *u* represents the total vectorial flow velocity that is obtained from the sum of the contributions of x, y, and z. The term Φ refers to the dissipation function, represented by Eq. (2.6) and μ is a viscosity term that relates the stresses to the volumetric deformation.

$$\nabla.(\rho u) = 0 \tag{2.1}$$

$$\nabla.(\rho u u) = -\frac{\partial p}{\partial x} + \nabla.(u\nabla u) + S_{Mx} \tag{2.2}$$

$$\nabla.(\rho v u) = -\frac{\partial p}{\partial y} + \nabla.(u\nabla y) + S_{My} \tag{2.3}$$

$$\nabla.(\rho w u) = -\frac{\partial p}{\partial z} + \nabla.(u\nabla w) + S_{Mz} \tag{2.4}$$

$$\nabla.\left(\rho c_p T u\right) = -p\nabla.u + \nabla.(k\nabla \mathrm{T}) + \Phi + S_i \tag{2.5}$$

$$\Phi = \mu\left\{2\left[\left(\frac{\partial u}{\partial x}\right)^2 + \left(\frac{\partial v}{\partial y}\right)^2 + \left(\frac{\partial w}{\partial z}\right)^2\right] + \left(\frac{\partial u}{\partial y} + \frac{\partial v}{\partial x}\right)^2 + \left(\frac{\partial u}{\partial z} + \frac{\partial w}{\partial x}\right)^2 \left(\frac{\partial v}{\partial z} + \frac{\partial w}{\partial y}\right)^2\right\} + \lambda(\nabla.u)^2 \tag{2.6}$$

The previous equations, written in differential form, describe energy, momentum and mass flow within an infinitesimal. Because of the turbulent nature of the flow, the solver used in this work considers and adapted version of these equations. The turbulence model used in the calculations presented in this work is the Reynolds-averaged Navier Stokes (RANS) equations.

And for the analysis present in this work, it is necessary to solve conservation equations for chemical species. Ansys Fluent predicts the local mass fraction of each species, Y_i, through the solution of a

convection-diffusion equation for the i th species. Equation 2.7 represents the general form of this conservation equation.

$$\nabla.(\rho\vec{v}Y_i) = -\nabla.\vec{J_i} + R_i + S_i \qquad 2.7$$

where R_i is the net rate of production of species i by chemical reaction and S_i is the rate of creation by addition from the dispersed phase plus any defined sources [Fluent]. The term $\vec{J_i}$ relates to the diffusion flux of species i, which arises because of gradients of concentration and temperature. The turbulent flow is considered to be turbulent inside the combustor. Ansys Fluent calculates the mass diffusion ($\vec{J_i}$) through the following equation:

$$\vec{J_i} = -\left(\rho D_{i,m} + \frac{\mu_t}{S_{ct}}\right)\nabla Y_i - D_{T,i}\frac{\nabla T}{T} \qquad 2.8$$

where S_{ct} is the turbulent Schmidt number, given by Eq.(2.9). $D_{i,m}$ is the mass diffusion coefficient for species i in the mixture, and $D_{T,i}$ is the thermal diffusion coefficient.

$$S_{ct} = \frac{\mu_t}{\rho D_t} \qquad 2.9$$

where μ_t is the turbulent viscosity and D_t the turbulent diffusivity.

3. ANALYSIS OF A SCRAMEJET COMBUSTION CHAMBER

The focus of this work is to study different phenomena and flow characteristics of the airflow inside a combustor chamber of a scramjet engine at Mach 6.8 and 30 km of altitude. This analysis considers different types of contour results of airflow variables and concentration of chemical reaction products as well as different the distribution of different properties along the walls to obtain the conclusions present in this paper. Figure 3.1 shows the computational domain of the combustor chamber. The sidewalls all present wall conditions, except the one further to the left that features symmetry condition in order to save computational resources. Four injections are present which consider pressure of 7 atm and Mach number 1 to inject H_2 as fuel in the supersonic flow. All the injections are perpendicular to the flow. The mesh features exactly 4132183 cells considering more refined regions near the walls to properly capture the physical effects inside the boundary layer. The model used in calculations considers 19 species in the chemical reactions and the turbulence model is the SST transition. 300 K wall temperature is considered in the calculations. Figure 3.2 presents the combustor chamber mesh in the injection region. The denser region on the upper wall is where the injectors are located.

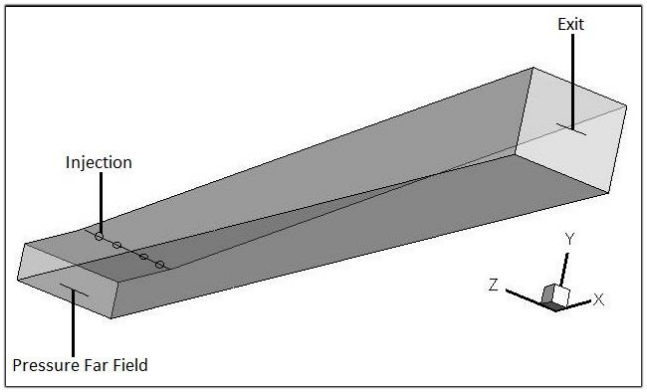

Figure 3.1 – Computational domain of the combustion chamber of a scramjet engine

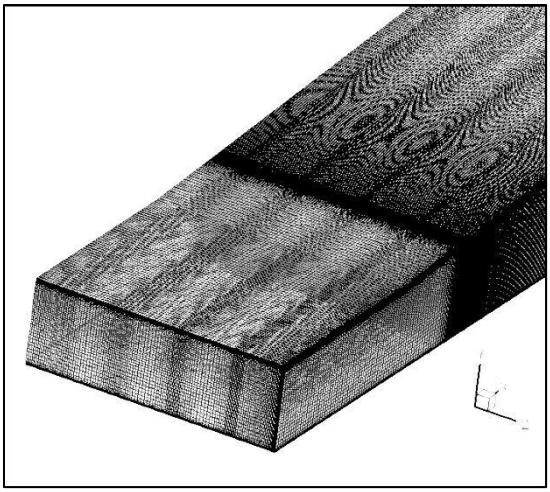

Figure 3.2 – Combustion chamber mesh.

3.1 – Mach number analysis

Figure 3.3 shows the Mach number contour inside the combustor chamber. It is important to highlight here that the boundary condition of the airflow entering in the combustor chamber was taken from a profile condition of the exit of the scramjet intake. That is, at first the calculations were performed considering only the intake of the engine. Once the result is obtained, it is imported the conditions at the intake exit and applied on the combustion chamber entrance. In this way, this simulation really works as the continuation of the scramjet intake calculation.
In Fig. 3.3 it is possible to see that in the combustor entrance there is a thicker boundary layer on the upper wall and a region of higher Mach number near the lower wall. Of course, the H_2 injections interfere the airflow. A region of low Mach number is created around the injectors. This region fades away as the airflow moves toward the exit; however, the Mach number is always higher near the lower wall.

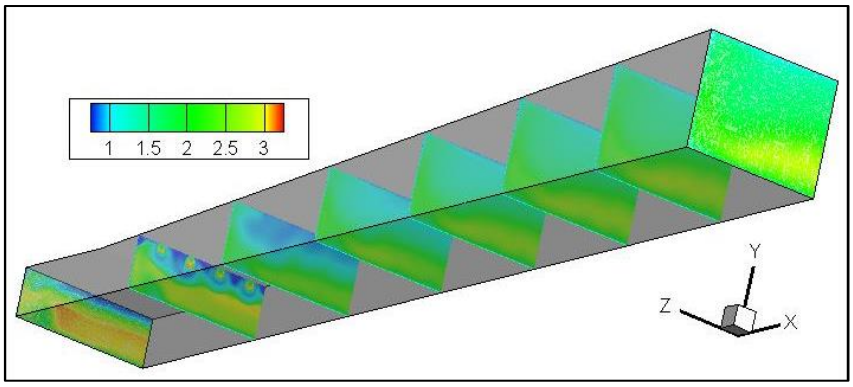

Figure 3.3 - Mach number contour of a combustion chamber.

3.2 – Static pressure analysis

The static pressure inside the combustor chamber is determinant to its performance. Figures 3.4, 3.5 and 3.6 present the static pressure contour and its distribution along the walls. It is possible to see in Figures 3.3 and 3.5 that the higher pressures happen in the injection. It is possible to see the influence of this high pressure until the following contour section. As the airflow goes toward the exit the overall pressure in the combustion chamber is the same.
In Figure 3.6 it is analyzed the pressure on the upper and lower walls. All the properties distributions on this work was considered in a line from the entrance until the exit on a region right on the second injection (from left to right). Before the injection, it is possible to see a pressure oscillation on both walls. That`s due to the reflected shock waves whose origin is the scramjet isolator. The H_2 injection into the supersonic airflow makes the pressure to go up mainly on the lower wall. The pressure on both walls gradually decreases as the airflow moves toward the exit.

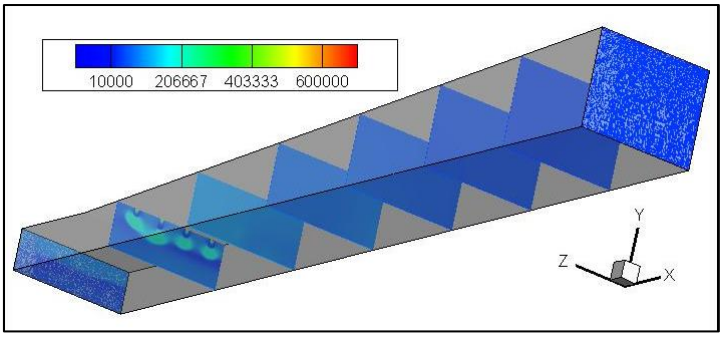

Figure 3.4 – Static pressure contour in a combustion chamber.

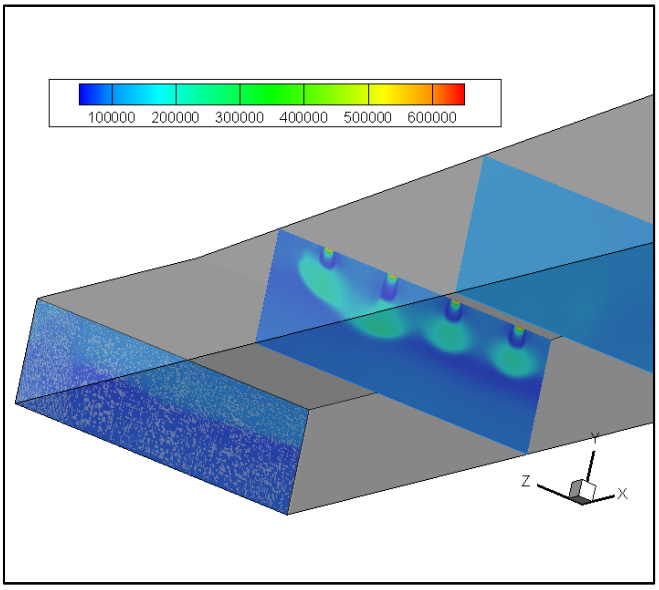

Figure 3.5 – Static pressure contour in the injection region.

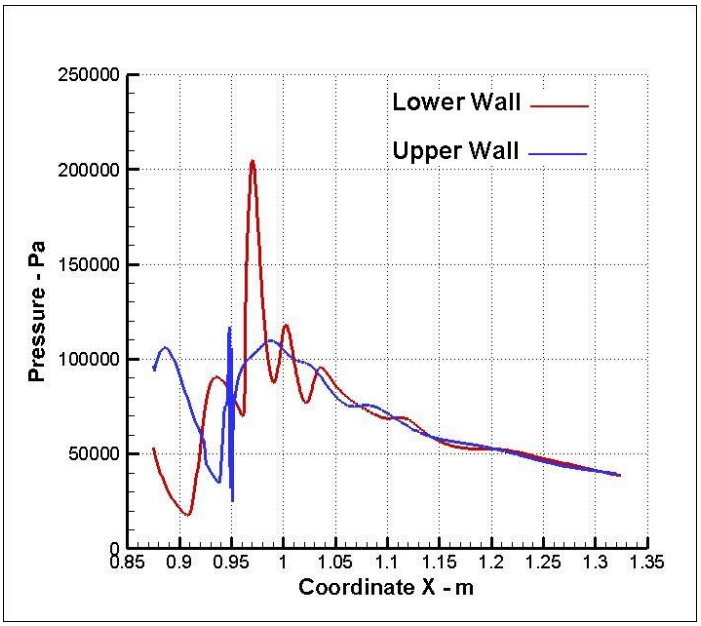

Figure 3.6 – Static pressure along the upper and lower walls of a scramjet combustion chamber.

3.3 – Static temperature analysis

Figures 3.7 and 3.8 show the temperature contour image and its distribution on the walls, respectively. At first, considering the contour image, it possible to see that higher temperature is seen in a region near the

upper wall in the combustor entrance. That certainly is due to the reflected shock wave that hits this region. The pressure analysis also showed that pressure increases in this region what reinforces the idea of a reflected shock wave impingement there. The H_2 is injected. The increase in temperature seen in the results show that the combustion reaction happens as soon as the H_2 starts mixing with the airflow. Higher temperatures are seen just after the injection in regions where certainly the H_2 is burned. Temperature in this region is around 2000 K.
Regarding the temperatures on the walls (upper and lower) presented in Figure 3.8, results show at first that there is higher temperature near the upper wall at the combustor entrance. This information is in accordance with was seen in the contour analysis. Both temperatures go down and suddenly increase as the fuel is injected. The great temperature decrease on the upper wall is because the fuel injection. The temperature then increases at the same rate as it decreased. It indicates that combustion happened in that region. Temperature on both walls then decreases and by 1.25 m it abruptly goes down. However, the upper wall always present higher temperature once the injection of H_2 happens on the upper wall.

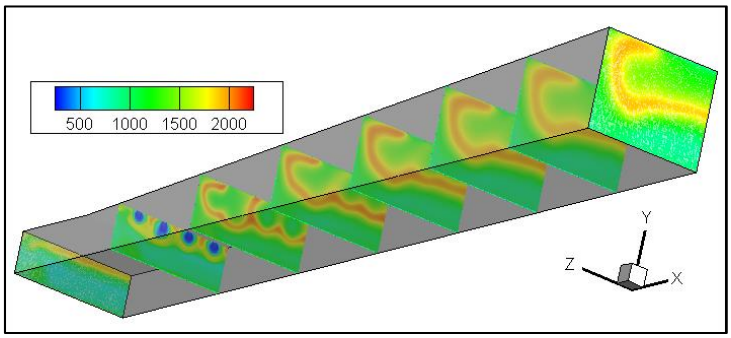

Figure 3.7 – Static temperature contour in a combustion chamber.

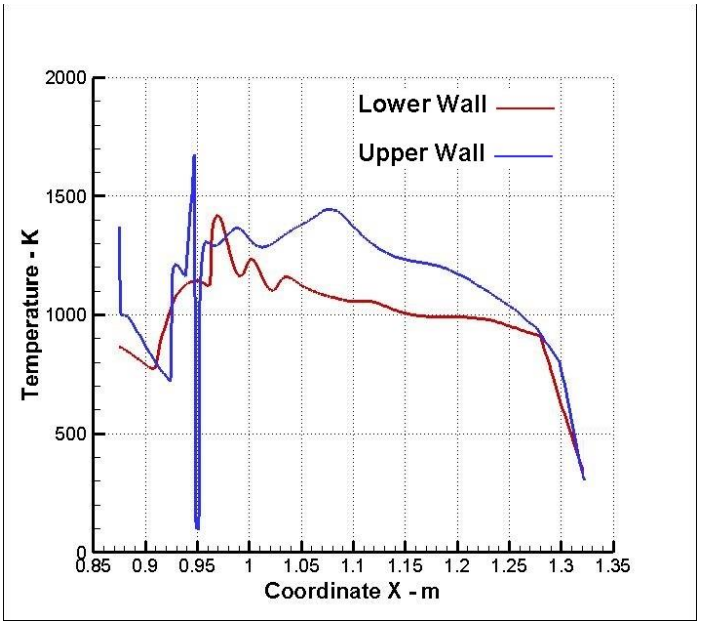

Figure 3.8 – Static temperature along the upper and lower walls of a scramjet combustion chamber.

3.4 – Mass fraction of H_2O and H_2

The contours of H_2O and H_2 mass fractions for a scramjet combustor chamber are shown in Figures 3.9 and 3.10, respectively. It is observed that water concentration is more near the upper wall of the chamber. As soon as the H_2 is injected water is created by the combustion process. The amount of water created gradually increases as the as the airflow goes toward the chamber exit. That certainly is related to the mixing of fuel and airflow. The greater the mixing the more efficient the combustion and consequently more water is created. The fact that there is no combustion in the area where H_2 is injected reinforces the importance of fuel mixing with the airflow.
Regarding the concentration of H_2 in the chamber, analysis of Figure 3.10 shows that, as expected, huge concentration is seen in the injection region and it soon starts mixing with the airflow and covers a greater

area of the chamber. This concentration of H_2, however, soon stops covering more area and remains the same until the exit of the combustion chamber whose some of its area does not present any concentration of H_2 and consequently any combustion process either, as it is seen in Figure 3.9.

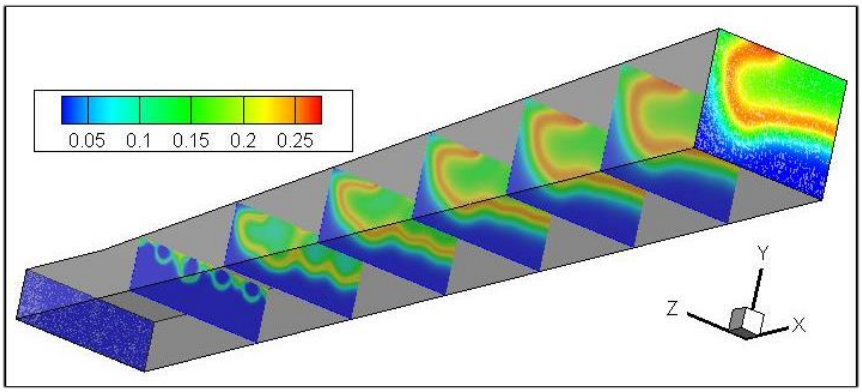

Figure 3.9 – Concentration of H_2O in moles inside the combustion chamber of a scramjet engine.

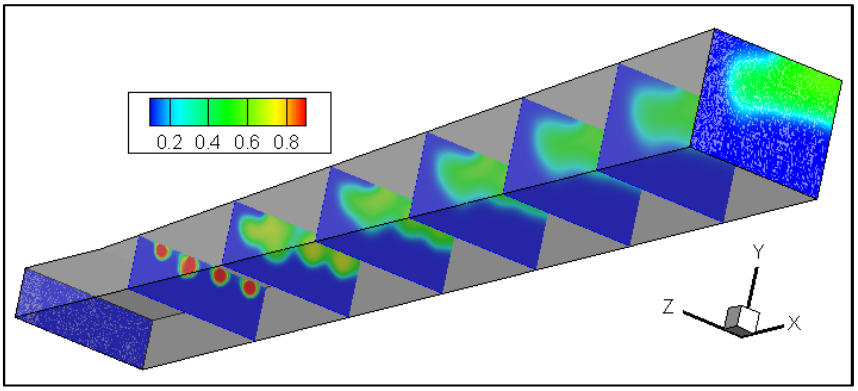

Figure 3.10 – Concentration of H_2 in moles inside the combustion chamber of a scramjet engine.

4. CONCLUSION

This CFD analysis has shown a good first overview of what happens inside a combustion chamber of a scramjet engine flying at Mach 6.8 and 30 km of altitude. Mach number contour shows that the fuel injection makes the airflow to decrease mainly in the region near the injection and as the airflow gets closer to the exit the Mach number becomes more homogenous at Mach number around 2. Regarding the static pressure, contour result shows that the greatest pressure happens in the injectors. The injection affects and increases the overall airflow pressure at the region but the pressure soon decreases and makes little effect by the exit of the chamber. By analyzing the static pressure distribution it was possible to state that, at first, the fuel injection makes the pressure to increase mainly on the lower wall. Further down towards the chamber exit, the pressure gradually starts to decrease and by 1.2 m the pressure on both wall reach 50000 Pa and remain the same. Considering the temperature, results show that the higher temperature occurs after the injections where combustion certainly happens. Temperature in this region is around 2000 K. The lowest temperature seen through contour image analysis is at the injector – less than 500 K. This is also seen in the temperature distribution along the upper wall. The temperature decrease happens only in the injection region. After it, combustion happens and the temperature increases. Gradually this temperature decreases and by the chamber exit it presents the same value on both walls: around 300 K. At last, analysis of concentration of H_2O and H_2 has been done. Results show that more H_2O is produced more by the end of the combustion chamber. That's certainly because near the injector the H_2 has not mixed well with the supersonic airflow and therefore combustion is not so efficient. The analysis of concentration of H_2 shows that the high concentration in the injection region is dispersed and almost the entire upper half of the chamber, at its exit, presents considerable concentration of H_2. On the other hand, the lower half of the chamber presents no fuel concentration.

5. ACKNOWLEDGMENTS

This work is part of a longstanding research program supported by the Brazilian Air Force. The technical support of the Institute of Advanced Studies (IEAv) is highly acknowledged. The financial support provided by the CAPES-PROAP program is also appreciated.

6. REFERENCES

LCAIDE, R. L. M. **Investigação da Combustão Supersônica em Túnel de Choque Hipersônico**. 2007. 97f. Thesis (Master in Science) – Instituto Tecnológico de Aeronáutica, São José dos Campos.

BARTH J. E, V. Wheatley, and M. K. Smart. **Hypersonic Turbulent Boundary-Layer Fuel Injection and Combustion: Skin-Friction Reduction Mechanisms**. In: AIAA J. 51.9 (2013), pp. 2147–2157. ISSN: 0001-1452.

BERTIN, J.J. **Hypersonic aerothermodynamics.** Washington, DC: AIAA, 1994. 608 p. (AIAA education series).

DOHERTY,L. J.; M. K. Smart, and D. J. Mee. **Design of an Airframe Integrated 3D Scramjet and Experimental Results at a Mach 10 Flight Condition**. In: 18th AIAA/3AF *Int. Sp. Planes Hypersonic Syst.* Technol. Conf. International Space Planes and Hypersonic Systems and Technologies Conferences. American Institute of Aeronautics and Astronautics, Sept. 2012.

GRIFFITHS, A. D. **Development and Demonstration of a Diode Laser Sensor for a Scramjet Combustor**. 2005. Thesis (Doctor of Philosophy) – The Australian Natonal University, Australia.

HEISER, W. H.; PRATT, D. T. **Hypersonic Airbreathing Propulsion**. Reston, VA: AIAA, 1994.

MOULE, Y.; V. Sabel'nikov, A. Mura, and M. K. Smart. **Computational Fluid Dynamics Investigation of a Mach 12 Scramjet Engine**. In: *J. Propuls. Power* 30.2 (2014), pp. 461–473. ISSN: 0748-4658.

SEGAL, C. **The Scramjet Engine: Process and Characteristics**. 1st ed. Cambridge: Cambridge University Press, 2009. 270 p.

SMART, M. Scramjets. In: **NATO/OTAN.RTO-EN-AVT-150**, Neuilly-sur-Seine, France: RTO, 2008, p. 1–38.

SMART, M and M. R. Tetlow. **Orbital Delivery of Small Payloads Using Hypersonic Airbreathing Propulsion**. In: J. *Spacecr. Rockets* 46.1 (2009), pp. 117–125. ISSN: 0022-4650.

TANIMIZU, K; David J. Mee, Raymond J. Stalker, and Peter A. Jacobs. **Drag force on quasi-axisymmetric scramjets at various flight Mach numbers: Theory and experiment**. In: *Shock Waves* 19.2 (2009), pp. 83–93. ISSN: 09381287.

7. RESPONSIBILITY NOTICE

The authors are the only responsible for the printed material included in this paper.